PFC/JA-86-18

The Anomalous Doppler Instability During Lower-Hybrid Current Drive

S.C. Luckhardt, A. Bers,
V. Fuchs,* and M. Shoucri*

March 1986

Plasma Fusion Center
Massachusetts Institute of Technology
Cambridge, Massachusetts 02139 USA

This work was supported in part by DOE Contract No. DE-AC02-78ET-51013 and in part by Hydro-Quebec Project No. 01844-571-59535.

Submitted for publication to The Physics of Fluids

*Projet Tokamak, IREQ, Varennes, Quebec, Canada JOL 2PO

THE ANOMALOUS DOPPLER INSTABILITY DURING LOWER-HYBRID CURRENT DRIVE

S.C. Luckhardt and A. Bers

Plasma Fusion Center, Massachusetts Institute of Technology
Cambridge, Massachusetts 02139, U.S.A.

and

V. Fuchs and M. Shoucri

Projet Tokamak, IREQ
Varennes, Quebec, Canada JOL 2PO

The anomalous Doppler instability is investigated for two-dimensional velocity distributions $f(v_{\|},v_{\perp})$ appropriate for lower-hybrid current drive. In this case, in contrast to the runaway electron problem, this mode becomes unstable at high density when the ratio $\omega_{pe}^2/\omega_{ce}^2$ is sufficiently large. Increasing the maximum velocity v_2 of the RF plateau, $v_1 \leq v_{\|} \leq v_2$, is also a destabilizing influence.

In this paper we give expressions for the growth rate of the electrostatic waves obeying the dispersion relation $\omega = \omega_{pe}(1 + \omega_{pe}^2/\omega_{ce}^2)^{-1/2}k_{\|}/k$, employing both analytic expressions for $f(v_{\|},v_{\perp})$ and numerical solutions for f from the two-dimensional Fokker-Planck equation. The analytical and numerical results are in close agreement.

I. INTODUCTION

In the present paper, we examine the nonrelativistic anomalous Doppler instability (ADI) of electron distributions which result from RF current drive. In plasmas with currents driven by RF waves, a velocity space anisotropy arises as a basic consequence of the current drive process. Thus, it is natural to look for possible destabilization of the anisotropy-driven modes. In the anomalous Doppler instability, electrostatic modes are driven unstable through interaction with fast electrons at the anomalous Doppler resonance velocity, $v_{\parallel} = v_{AD} = (\omega_{ce} + \omega)/k_{\parallel}$, where ω_{ce} is the electron cyclotron frequency, $k_{\parallel}$ is the parallel wavenumber, and ω is the frequency of the unstable wave. This instability is well-known to play an important role in the low density runaway electron regime of tokamak operation, and considerable theoretical work has elucidated the characteristics of this mode using electron velocity distribution functions, $f_e(v_{\parallel}, v_{\perp})$, appropriate for the runaway electron tail (see Ref. 1 and references contained therein). In the case of RF current drive the growth rate and marginal stability condition of this mode was calculated earlier[2] using a simple model for the RF driven distribution function. Here we use a more sophisticated model that is an approximate analytical solution to the 2D Fokker-Planck equation,[3] and then make comparisons to results from the full numerical solution of the Fokker-Planck equation.

As far as the ADI is concerned, there are three principal differences between the runaway problem and the RF current drive problem, which stem from the form of the raised plateau of $F(v_{\parallel}) = \int f_e 2\pi v_{\perp} dv_{\perp}$ in the velocity space region $v_1 \leq v_{\parallel} \leq v_2$ in which the externally injected spectrum of waves causes substantial quasi-linear diffusion. First, for strong RF diffusion, the slope of $F(v_{\parallel})$ on the RF plateau is smaller than the slope of the corresponding distribution function for a runaway tail near the critical runaway velocity. Hence, Landau damping of the unstable waves will be weaker in the RF case.

Second, the RF-generated plateau height is generally larger than the runaway tail height for typical tokamak experiments, thus contributing a correspondingly larger effect from the anomalous Doppler resonance. And third, the upper velocity limit of the plateau, v_2, is generally smaller than the maximum velocity of the runaway tail. This latter difference will result in a substantial difference in the density regime for which instability is expected. In particular, we will show that in the RF current drive case, the parameter $y = \omega_{pe}/\omega_{ce}$ must exceed a minimum value (typically ~ 0.3) before instability can occur.

The electrostatic plasma waves of interest are described by the nonrelativistic dispersion function $D(\bar{k},\omega)$.[4]

$$D(\bar{k},\omega) = 1 + \sum_j \sum_n \frac{\omega_{pj}^2}{k^2} \int d^3v \, \frac{J_n^2(k_\perp v_\perp/\omega_{cj})}{\omega - k_\parallel v_\parallel - n\omega_{cj} + i\gamma} \, D_{nj} f_j(v_\parallel, v_\perp) \tag{1}$$

for a uniform magnetized plasma, where j = e, i (electrons, ions), and n runs through $n = 0, \pm 1, \pm 2, \ldots$. Further,

$$\omega_{pj}^2 = 4\pi n_j e_j^2/m_j, \quad \omega_{cj} = |e_j B/m_j c|. \tag{2}$$

J_n is the ordinary Bessel function of order n, and the operator D_{nj} is given by:

$$D_{nj} = \frac{n\omega_{cj}}{v_\perp} \frac{\partial}{\partial v_\perp} + k_\parallel \frac{\partial}{\partial v_\parallel}, \tag{3}$$

and $f_j(v_\parallel, v_\perp)$ is the velocity distribution function. The dispersion relation and the growth rate are, respectively,

$$\mathrm{Re}(D) = 0, \quad \gamma = -\,\mathrm{Im}(D)/(\partial \mathrm{Re}(D)/\partial\omega)\Big|_{\mathrm{Re}(D)\,=\,0} \tag{4}$$

Provided that $k_\perp^2/k_\parallel^2 \ll m_i/m_e$, we can neglect the ion contributions in (1), and, for $\omega^2 \ll \omega_{UH}^2 = \omega_{pe}^2 + \omega_{ce}^2$, we get the dispersion relation:

$$\frac{\omega^2}{\omega_{ce}^2} \cong \frac{k_\parallel^2}{k^2}\,\frac{y^2}{1+y^2}, \qquad y = \frac{\omega_{pe}}{\omega_{ce}}. \tag{5}$$

The corresponding most general form of the growth rate for an arbitrary distribution function is:

$$\gamma = \sum_n \frac{\pi^2\omega\omega_{pe}^2}{k^2|k_\parallel|}\,A \int_0^\infty v_\perp dv_\perp\, J_n^2\left(\frac{k_\perp v_\perp}{\omega_{ce}}\right) D_{ne}\, f_e(v_\perp, v_{\parallel n}), \tag{6}$$

where $v_{\parallel n} = (\omega - n\omega_{ce})/k_\parallel$ are the resonant values of $v_\parallel$, and the factor $A = \left(1 - \frac{\omega^2}{\omega_{ce}^2}\right)\left(1 + y^2 - \frac{\omega^2}{\omega_{ce}^2}\right)^{-1}$ arises from the evaluation of $\partial \mathrm{Re}(D)/\partial\omega$ discussed in the Appendix. In the following calculations, normalized variables are used according to:

$$v \to v/v_e \text{ with } v_e^2 = T_e/m_e, \quad \omega \to \omega/\omega_{ce}, \quad \gamma \to \gamma/\omega_{ce}, \quad k \to kv_e/\omega_{ce}. \tag{7}$$

Of the terms in (6), only the $n = 0, \pm 1$ resonance terms need to be retained; the other resonances occur in regions where f is negligibly small. Conventionally these three resonances are called the Landau ($n = 0$), the anomalous Doppler ($n = -1$), and the Doppler cyclotron ($n = 1$) resonances. The resonant velocities are, respectively:

$$v_L = \frac{\omega}{k_\parallel}, \quad v_{AD} = \frac{\omega + 1}{k_\parallel}, \quad v_{DC} = \frac{\omega - 1}{k_\parallel}, \tag{8}$$

and we label their contributions in Eq. (6) as γ_L, γ_{AD}, and γ_{DC}, respectively. The growth rate (6) then becomes:

$$\gamma = \sum_{n=0,\pm1} 2\pi G \int_0^\infty v_\perp dv_\perp \, J_n^2(k_\perp v_\perp) \, D_n \, f(v_\perp, v_{\parallel n}), \tag{9a}$$

where

$$G = \frac{\pi}{2} \frac{\omega}{k^2} y^2 \frac{(1 - \omega^2)}{(1 + y^2 - \omega^2)} \tag{9b}$$

$$D_n f = \frac{\partial f}{\partial v_\parallel} \, \mathrm{sign}(k_\parallel) + \frac{n}{v_\perp |k_\parallel|} \frac{\partial}{\partial v_\perp} f. \tag{10}$$

It can be seen from Eqs. (9) and (10) that γ_{AD} becomes large and positive when $|\partial f/\partial v_\parallel| \ll |\partial f/\partial v_\perp|$ at the resonance velocity $v_\parallel = v_{AD} = (\omega_{ce} + \omega)/k_\parallel$. Thus, the low phase velocity electrostatic waves can interact with energetic electrons via the anomalous Doppler resonance, and, due to the anisotropy in the RF-created electron distribution function $f(v_\perp, v_\parallel)$, this resonance contributes the positive term, γ_{AD}, to the overall growth rate of the wave.

II. NECESSARY CONDITIONS FOR INSTABILITY

The two-dimensional electron distribution function for RF current drive is shown schematically in Figure 1. The velocities of electrons resonant with

the wave are also indicated; the important resonances are $v_{AD} = (\omega + 1)/k_{\|}$, $v_{DC} = (\omega - 1)/k_{\|}$, and $v_L = \omega/k_{\|}$. Instability occurs when the magnitude of the sum of the two damping rates, $|\gamma_L + \gamma_{DC}|$, is less than the growth rate γ_{AD} at the anomalous Doppler resonance. We can obtain necessary conditions for instability by examining limiting cases where each of the damping rates is small and the growth term is maximum. The damping rate γ_L is obviously relatively small when the wave phase velocity falls into the plateau region, that is, when the inequality $\omega/k_{\|} > v_1$ is obeyed. On the other hand, if $\omega/k_{\|} \lesssim v_1$, then waves will suffer heavy Landau damping owing to the rapid transition of $f(v_{\perp},v_{\|})$ to the Maxwellian bulk at $v_{\|}$ values below v_1. The growth rate due to the anomalous Doppler resonance will be largest when $v_{AD} = (\omega + 1)/k_{\|}$ is less than v_2, that is, when the inequality $k_{\|}v_2 > \omega + 1$ is obeyed. If $v_{AD} > v_2$, then γ_{AD} will be small or negative, which follows from the fact that for $v_{\|} > v_2$ RF diffusion is absent, so that pitch angle scattering will tend to isotropize $f(v_{\|},v_{\perp})$ along contours of constant energy, $v_{\|}^2 + v_{\perp}^2 =$ constant. Evidently, the above two inequalities are necessary conditions for instability. The Doppler cyclotron resonance affects particles with $v_{\|} < 0$, Figure 1. In this region, we have $D_{RF} = 0$, and f will be dominated by pitch angle scattering. For $v_{DC} \gtrsim - v_1$, the Doppler cyclotron resonance may fall into the bulk causing significant damping of the waves on the thermal particles. Hence, $v_{DC} < - v_1$, or $\omega \lesssim - v_1 k_{\|} + 1$, is roughly an additional necessary condition for instability, assuming there is no backward going RF current. These three necessary conditions for instability are tabulated in Table I and are represented as lines in $(\omega,k_{\|})$-space in Fig. 2. The dispersion relation places a further constraint on the wave-frequency, namely, $\omega \lesssim \omega^{max} = y(1 + y^2)^{-\frac{1}{2}}$, also listed in Table I; the line ω^{max} is shown in Fig. 2. For suitable values of v_1, v_2, and y it is possible to satisfy all three

conditions in a particular region of the $(\omega,k_{||})$ plane, the shaded region in Fig. 2. Waves with ω and $k_{||}$ in this region are potentially unstable. Clearly, if the parameter $y=\omega_{pe}/\omega_{ce}$ is sufficiently small, the unstable region of $(\omega,k_{||})$-space vanishes, and all wave modes would be stable. Thus, we expect instability only in plasmas with sufficiently high density, i.e., having large enough y.

The $(\omega,k_{||})$ representation is useful for quickly determining if any set of experimental conditions, as given by y, v_1, and v_2, is favorable or unfavorable for instability.

The necessary conditions for wave growth (the inequalities given in Table I) can be combined to give the two conditions,

$$v_2 > 3\ v_1 \tag{11}$$

and

$$y^2 \equiv \omega_{pe}^2/\omega_{ce}^2 > \frac{1}{(v_2/v_1 - 1)^2 - 1}, \tag{12}$$

for the existence of an unstable region in $(\omega,k_{||})$-space. Evidently, increasing the values of v_2 and y are destabilizing influences.

The conditions (11) and (12) will be modified by relativistic effects. The relativistic generalization of the anomalous Doppler resonance condition is:

$$v_{||} = v_{AD} = \frac{\omega_{ce}/\gamma + \omega}{k_{||}}, \tag{13}$$

where $\gamma = (1 - v^2/c^2)^{1/2}$ and $\omega_{ce} = |eB/mc|$ is the nonrelativistic cyclotron frequency. Combining (13) with the other inequalities in Table I and neglecting $v_{\perp}^2/c^2$ gives, instead of (11) and (12),

$$\frac{v_2}{v_1} > 1 + \frac{2}{\gamma_2} \tag{14}$$

and

$$y^2 > \frac{1}{\gamma_2^2(v_2/v_1 - 1)^2 - 1}, \tag{15}$$

where $\gamma_2 = (1 - v_2^2/c^2)^{-1/2}$ for the necessary conditions for instability. It can be seen that the relativistic effects tend to be destabilizing since $\gamma^2 > 1$. This is clear also in Figure 2, where the dashed ine is the anomalous Doppler resonance line for the case $\gamma_2 > 1$. The AD line moves to the left as γ_2 increases, hence the allowed zone of unstable waves increases.

In the following, the preceding considerations based on physical arguments are verified in the nonrelativistic limit, by explicit calculation of γ_L, γ_{AD}, and γ_{DC} for model distribution functions, and for numerically computed two-dimensional solutions of the Fokker-Planck equation. The above picture is useful for identifying the parameter ranges in which the anomalous Doppler instability can exist; however, to ascertain the importance of this instability, the growth rate (6) must be evaluated.

III. DISTRIBUTION FUNCTION

The distribution function of interest is produced by a combination of quasilinear diffusion from the externally applied RF waves and of collisional processes, energy drag and diffusion, and pitch angle scattering.

In the resonant region $v_1 < v_{\|} < v_2$, where the externally imposed spectrum of RF waves causes quasilinear diffusion, an RF plateau (Figure 1) is formed. On the plateau, thermal particles are pulled out from the bulk and rapidly quasilinearly diffused and simultaneously pitch angle scattered to large values of $v_{\perp}$. The distribution function, $\tilde{f} = f - f_m$, where f_m is the bulk Maxwellian, is therefore broadened in the perpendicular direction.

The Fokker-Planck equation describing this distribution function f is:

$$\bar{\nabla}_v \cdot \bar{S} = 0, \tag{16}$$

where the components of the velocity space flux $\bar{S}$, parallel and perpendicular to the magnetic field, are:

$$S_{\|} = - Bf \frac{v_{\|}}{v^3} - \frac{\partial f}{\partial v_{\|}} \left[D + \frac{A}{2} \frac{v_{\perp}^2}{v^3} + B \frac{v_{\|}^2}{v^5} \right] + \frac{\partial f}{\partial v_{\perp}} \frac{v_{\perp} v_{\|}}{v^3} \left[\frac{A}{2} - \frac{B}{v^2} \right], \tag{17}$$

$$S_{\perp} = - Bf \frac{v_{\perp}}{v^3} + \frac{\partial f}{\partial v_{\|}} \frac{v_{\perp} v_{\|}}{v^3} \left[\frac{A}{2} - \frac{B}{v^2} \right] - \frac{\partial f}{\partial v_{\perp}} \frac{1}{v^3} \left[\frac{A}{2} v_{\|}^2 + B \frac{v_{\perp}^2}{v^2} \right]. \tag{18}$$

The normalized velocity variable, $v \to v/v_e$, where $v_e = (T_e/m)^{1/2}$, is used. The coefficients $A \cong 1 + Z_i$ and $B \cong 1$ are discussed in Ref. 3, and $D = D_{QL}/\nu_o v_e^2$, with $\nu_o = 4\pi n_e^2 e^4 \ln\Lambda / m_e^2 v_e^3$. For a given form of the quasilinear diffusion coefficient D, the solution of (16) can be carried out numerically, as discussed in Ref. 3. In section V of this paper, we calculate growth rates using the numerical solution of Eq. (16). To obtain analytical results for the growth rates, we will use the approximate analytical form for f presented in Ref. 3.

The analytical distribution function is written in terms of the bulk Maxwellian, f_m, and a population of suprathermal electrons $\tilde{f}$:

$$f = f_m + \tilde{f}. \tag{19}$$

The normalized Maxwellian is:

$$f_m = (2\pi)^{-3/2} \exp(-v^2/2), \tag{20}$$

and the distribution function of the suprathermal particles is:

$$\tilde{f} = \frac{\tilde{F}(v_\parallel)}{2\pi\tilde{T}_\perp(v_\parallel)} \exp(-v_\perp^2/2\tilde{T}_\perp), \tag{21}$$

where the quantities entering (21) are related to the perpendicular velocity moments of f according to:

$$\tilde{F} = 2\pi \int_0^\infty v_\perp dv_\perp \tilde{f}, \quad \tilde{T}_\perp = \frac{2\pi}{2\tilde{F}} \int_0^\infty v_\perp^3 dv_\perp \tilde{f}. \tag{22}$$

The form (21) for $\tilde{f}$ is substantiated by the two-dimensional numerical results discussed in Ref. 3.

The plateau perpendicular temperature, because of pitch angle scattering, is much greater than the temperature of the bulk. In our normalizations, $T_\perp \equiv T_p >> 1$, with $T_\perp = 1$ for the bulk particles, f_m. The perpendicular temperature, T_p, of the suprathermal component depends on the limits of the resonant region, v_1 and v_2, and on the ion charge, Z_i. Following Ref. 3, we have:

$$T_p \cong \frac{\dfrac{v_2^{\alpha+1} - v_1^{\alpha+1}}{\alpha + 1} - (v_2 - v_1)v_1^{\alpha}}{2(v_2 - v_1)v_1^{\alpha-2} - \dfrac{v_2^{\alpha-1} - v_1^{\alpha-1}}{\alpha - 1}}, \tag{23}$$

where

$$\alpha = 2(1 + Z_i)/(2 + Z_i). \tag{24}$$

An approximate analytical solution to (16) can be obtained in the region $v_1 < v_{\|} < v_2$, where D is sufficiently large. A moment equation approach is used, and Ref. 3 gives:

$$\frac{F'(v_{\|})}{F(v_{\|})} = \frac{-v_{\|}\left[\dfrac{1 + Z_i}{a_1} + 1 - \dfrac{2}{v_{\|}^2 a_5}\right]}{Da_3 v_{\|}^3 + (1 + Z_i)T_{\perp}/a_1 + a_3/a_5} \equiv -v_{\|}H(v_{\|}), \tag{25}$$

where $a_n = 1 + nT_{\perp}/v_{\|}^2$, and Z_i is the ion charge. For the calculations of the growth rates in the next section, we do not solve the differential equation (25) explicitly, but rather we use (25) to calculate the derivative $F'(v_{\|})$ for a plateau height, $F(v_{\|})$, determined self-consistently with the total RF-driven current, J_{RF}. We can do this because, for RF power levels of interest, D is relatively large ($D > 1$), and the plateau is consequently rather flat (typically a few percent change in $\bar{f}$ from $v_{\|} = v_1$ up to $v_{\|} = v_2$). The plateau height itself can be estimated using the approximation[3]

$$F_p \cong \frac{F_m(v_1)}{1 - \exp\left(- \frac{(A + B)}{AT_p + B} v_1^2/2 \right)}. \tag{26}$$

Our procedure then is to take the experimental value of J, determine the plateau height from the equality, $J = \int_{-\infty}^{\infty} v_{\|} dv_{\|} \; F(v_{\|})$, and self-consistently choose v_1 according to Eq. (26). We use this procedure in deriving the data of Table II, where the theory parameters v_1, $T_{\perp}$, and F_p, the plateau height, are obtained for the given experimental conditions.

The described procedure is sufficient to give an explicit analytical form for $\bar{f}$ in the region $v_1 < v_{\|} < v_2$ for any given set of experimental conditions, J, v_2, and T_e. In the region $v_{\|} > v_2$, pitch angle scattering dominates, and the steady state solution is highly isotropic with $\bar{f} \sim \exp[- (v_{\perp}^2 + v_{\|}^2)/2T_p]$. In the region $v_{\|} < 0$, the thermal Maxwellian component dominates over the population of hot electrons pitch angle scattered from the plateau. The backward-going hot electron component ($v_{\|} < 0$) does not, in most circumstances, significantly contribute to the growth rates, as will be shown in the calculations with the full 2-D numerical distribution function.

IV. ANALYTICAL GROWTH RATES

The growth rates (9) will first be evaluated using the distribution function given in the form of Eq. (21). The growth rate as a function of the characteristic quantities $T_{\perp}(v_{\|})$ and $F'(v_{\|})$ will be given explicitly. Only two types of integrals occur in the evaluation of Eq. (9), namely,

$$\int_0^\infty x dx\, J_n^2(\alpha x)\, e^{-\rho x^2} = \frac{1}{2\rho}\, e^{-\alpha^2/2\rho}\, I_n(\alpha^2/2\rho) \equiv P_n(\alpha,\rho), \text{ and} \tag{27a}$$

$$\int_0^\infty x^3 dx\, J_n^2(\alpha x)\, e^{-\rho x^2} = -\frac{\partial}{\partial\rho} P_n(\alpha,\rho), \tag{27b}$$

where the I_n are the modified Bessel functions. Terms of all order in $k_\perp \rho_{ce}$ are retained; ρ_{ce} is the gyroradius, $v_\perp/\omega_{ce}$. We find, for $k_\parallel > 0$:

$$\gamma_L = G \left\{ W_0(q) \left[F' + F \frac{T_\perp'}{T_\perp} q \left(\frac{I_1}{I_0} - 1 \right) \right] \right\}_{v_\parallel = v_L}, \tag{28}$$

$$\gamma_{AD} = G \left\{ W_1(q) \left[F' + F \frac{T_\perp'}{T_\perp} \left(q \frac{I_0}{I_1} - q - 1 \right) + \frac{F}{T_\perp k_\parallel} \right] \right\}_{v_\parallel = v_{AD}}, \tag{29}$$

$$\gamma_{DC} = G \left\{ W_1(q) \left[F' + F \frac{T_\perp'}{T_\perp} \left(q \frac{I_0}{I_1} - q - 1 \right) - \frac{F}{T_\perp k_\parallel} \right] \right\}_{v_\parallel = v_{DC}}, \tag{30}$$

where

$$G = \frac{\pi}{2} \frac{\omega}{k^2} y^2 \frac{(1 - \omega^2)}{(1 + y^2 - \omega^2)}, \tag{31}$$

v_L, v_{AD}, and v_{DC} are the resonant velocities defined in Eq. (8), $W_n(q) = I_n(q) \exp(-q)$, and the argument of the modified Bessel functions is:

$$q = k_\perp^2 T_\perp(v_\parallel). \tag{32}$$

If the anomalous Doppler resonance is on the plateau ($v_{AD} < v_2$), the dominant contribution to γ_{AD} comes from the term $F/T_\perp k_\parallel$ in Eq. (29). Thus, when $v_1 < v_{AD} < v_2$, γ_{AD} will provide a positive contribution to the

growth rate. In the region $v_{\|} > v_2$, $\tilde{f}$ is comparatively isotropic: $\tilde{f} \sim \exp[-(v_{\|}^2 + v_{\perp}^2)/2T_{\perp}]$, with $T_{\perp}' \cong 0$, so that γ_{AD} reduces to:

$$\begin{aligned}\gamma_{AD} &\cong GW_1(q)F(v_{\|})\Big|_{v_{\|}=v_{AD}} \left[\frac{F'}{F} + \frac{1}{T_{\perp}k_{\|}}\right]\Big|_{v_{\|}=v_{AD}} \\ &\cong GW_1(q)F(v_{\|})\Big|_{v_{\|}=v_{AD}} \left[-\frac{\omega + 1}{k_{\|}T_{\perp}} + \frac{1}{T_{\perp}k_{\|}}\right] \\ &= -\frac{G}{k_{\|}T_{\perp}} W_1(q)F(v_{\|})\Big|_{v_{\|}=v_{AD}} < 0. \end{aligned} \tag{33}$$

Hence, no growth can occur for $v_{AD} > v_2$.

The Landau contribution is clearly negative since $F' < 0$ for these waves, as is the Doppler cyclotron growth rate, γ_{DC}. The γ_{DC} term comes from resonance with electrons with $v_{\|} = v_{DC} = (\omega_{ce} - \omega)/k_{\|} < 0$. Generally, γ_{DC} will be small unless v_{DC} moves into the bulk region, $v_{DC} > -4$, or if an RF plateau is formed in the negative $v_{\|}$ direction. This latter possibility can occur under experimental conditions where usually a fraction of the RF wave power propagates opposite to the main power flow, generating a small current opposing the main current. Here, we will neglect this effect.

Now, the individual contributions γ_L, γ_{AC}, and γ_{DC} can be evaluated using the analytical expression (25), recalling that:

$$F = F_m + \tilde{F}, \tag{34}$$

where the parallel Maxwellian is $F_m = (2\pi)^{-1/2} \exp(-v_{\|}^2/2)$. First, we deal with the Landau damping term (29).

Landau Damping

The Maxwellian part of $F_{\|}$ immediately gives, on substitution into Eq. (28):

$$\gamma_L^{(m)} = - G \left[W_o(q)\, v_{\|}\, F_m(v_o) \right] \Big|_{v_{\|}=v_L}, \tag{35}$$

where $q = k_{\perp}^2$, since $T_{\perp} = 1$ for the bulk Maxwellian. The suprathermal part of the distribution, $\tilde{F}$, has $T_{\perp} = T_p$, by Eq. (23), and on the plateau, with $\tilde{F}'$ given by Eq. (25), we get:

$$\gamma_L^{(P)} = - G \left[W_o(q)\, v_{\|}\, F(v_{\|})\, H(v_{\|}) \right] \Big|_{v_{\|}=v_L}, \tag{36}$$

where we have neglected terms proportional to $T_{\perp}'/T_{\perp}$, and the function H is defined in Eq. (25).

Anomalous Doppler Growth

The anomalous Doppler term in the growth rate (27) can be evaluated in a similar way. The contribution from the Maxwellian F_m is:

$$\gamma_{AD}^{(m)} = - G \left[W_1(q)\, v_{\|}\, F_m(v_{\|}) \right] \Big|_{v_{\|}=(\omega + 1)/k_{\|}}, \tag{37}$$

which is negative definite, but is obviously extremely small in cases of interest since $v_{AD} = (\omega + 1)/k_{\|}$ is much larger than the bulk thermal velocity, v_e. The factor $F_m(v_D)$ is thus very small compared to the Landau damping term in Eq. (35).

In contrast, the contribution of the suprathermals is destabilizing on the plateau, where, upon neglecting the small terms with $T_\perp'$ and F', we get:

$$\gamma_{AD}^{(p)} = G(v_{AD} - v_L) \frac{\tilde{F}}{T_p} [\, W_1(q) \,] \Big|_{v_\parallel = v_{AD}}. \tag{38}$$

In Eq. (38), we note that $v_{AD} > 2v_L$, which follows from the definition of v_{AD} and v_L and the wave dispersion relation. Using these relations we find:

$$\frac{v_{AD}}{v_L} \geq 1 + \frac{(1 + y^2)^{1/2}}{y}. \tag{39}$$

Outside the RF region for $v_\parallel > v_2$, $f(v_\parallel, v_\perp)$ is defined by pitch angle scattering effects, and, as discussed in section III, we have:

$$\tilde{F}(v_\parallel > v_2) \cong F_p \exp\left[- \frac{v_\parallel^2}{2T_p} (1 + B/A) \right], \tag{40}$$

which, when substituted into Eq. (29), immediately gives:

$$(\gamma_{AD})_{v_\parallel > v_2} \cong - G \frac{(v_L + v_{AD}\, B/A)}{T_p} [\, W_1(q)\, \tilde{F} \,] \Big|_{v_\parallel = v_{AD} > v_2}. \tag{41}$$

This expression is negative definite, and because all other terms contributing to γ are also negative it follows that instability cannot occur when $v_\parallel > v_2$. This result was to be expected since the distribution function with $v_\parallel > v_2$ is nearly isotropic.

Doppler Cyclotron Term

Finally, we consider the effects of the Doppler cyclotron resonance ($n = +1$) located at $v_{\|} = v_{DC} = (\omega - \omega_{ce})/k_{\|}$. Since waves of interest have $\omega < \omega_{ce}$ and $k_{\|} > 0$, v_{DC} will lie in the negative $v_{\|}$ region and will become significant when v_{DC} approaches the thermal bulk, i.e., $v_{DC} \cong - 4\ v_e$. The contribution originating from the Maxwellian background due to the DC resonance is negative definite and is given by:

$$\gamma_{DC}^{(m)} = - G \left[W_1(q)\ |v_{\|}|\ F_m \right] \Big|_{v_{\|}=v_{DC}}, \tag{42}$$

where:

$$v_{DC} = (\omega - 1)/k_{\|} = 2\ v_L - v_{AD} < 0. \tag{43}$$

This contribution to the total damping can become significant for small (i.e., bulk) values of $|v_{DC}|$, which is possible only for waves with frequencies $\omega \gtrsim \omega_{ce}/2$. The latter condition follows from the fact that $- v_{DC} = v_L(\omega_{ce}/\omega - 1)$ and that $v_L \gtrsim 4\ v_e$ for waves of interest, and hence the requirement for Doppler cyclotron damping on the bulk, $- v_{DC} \lesssim 4\ v_e$, implies that $\omega \gtrsim \omega_{ce}/2$. Waves in this frequency range are allowed by the dispersion relation only if y is sufficiently large, that is, $y \cong 0.5 \rightarrow 1.0$. The Doppler cyclotron contribution to γ, therefore, must be included in the case of high density plasmas, with $y \cong 1$.

The relevant contributions to γ from both the thermal and suprathermal particles can now be written as:

$$\gamma = \gamma_L^{(m)} + \gamma_{DC}^{(m)} + \gamma_L^{(p)} + \gamma_{AD}^{(p)}, \tag{44}$$

where the individual terms are given by Eqs. (35), (36), (38), and (42). The expression for γ_{AD} in Eq. (38) applies when $v_{AD} < v_2$. In the case where $v_{AD} > v_2$, γ_{AD} is negative definite and no growth is possible.

The numerical values of γ can now be calculated as a function of the wave parameters ω and $k_\parallel$ for a given set of experimental conditions: y^2, v_2, J, T_e, etc.

V. GROWTH RATES FOR VERSATOR II

As an example, we will now apply the results of the preceding section to calculate the growth rates for a set of conditions typical of the Versator II current drive experiment.[5] The parameters for six cases tabulated in Table II are chosen to simulate an experiment in which the density is varied while keeping the RF-driven current and toroidal field constant.

In this example, we take $B_{toroidal}$ = 1.2 Tesla, T_e = 200 eV, J = 390 A/cm^2, f_0 = 2.45 GHz, Z_{eff} = 3, and the density is varied in the six cases of Table II. The velocity v_2 is the highest phase velocity of the RF power spectrum, and is limited by the accessibility condition, $n_\parallel = ck_\parallel/\omega \geq n_\parallel^{ACC}$. For the slow lower hybrid wave, $n_\parallel^{ACC} = (1 + \omega_{pe}^2/\omega_{ce}^2 - \omega_{pi}^2/\omega^2)^{1/2} + \omega_{pe}/\omega_{ce}$. In Table II, v_2 is taken to be $c/n_\parallel^{ACC}$; hence v_2 changes for each value of the density. In Table II, velocities are normalized to the thermal velocity, $v_e = (T_e/m)^{1/2} = 6 \times 10^8$ cm/sec.

The remaining parameters of the distribution function, T_p, F_p (the plateau height), and v_1 are calculated using the formulas, (23) and (26),

and definition, $J = \int v_{\|} dv_{\|} F(v_{\|})$, where J is the current density normalized to $en_e v_e$.

In case (d) of Table II, we have $n = 1 \times 10^{13}$ cm^{-3}, $\omega_{pe}^2/\omega_{ce}^2 = y^2 = 0.694$, $J = 0.41\ en_e v_e$, and $v_z = 23.8\ v_e$. Using the formulae of section III, we find that $T_p = 82\ T_{bulk}$, $F_p = 1.44 \times 10^{-3}$, and $v_1 = 4\ v_e$, as given in Table II.

The growth rates $\gamma(\omega, k_{\|})$ calculated from Eq. (44) are plotted in Figures 3(a)-(f), corresponding, respectively, to the cases (a)-(f) of Table II. For example, in Figure 3(d), $n = 1 \times 10^{13}$, and we show ten equally spaced contours of γ = constant ≥ 0. These contours extend from the marginal stability limit, $\gamma = 0$, to $\gamma = \gamma_{max} = 1.82 \times 10^{-3}\ \omega_{ce}$. The fastest growing wave has a frequency of $\omega = 0.38\ \omega_{ce}$ and $k_{\|} = 5.8 \times 10^{-2}\ \omega_{ce}/v_e$, as seen in Figure 3(d). These values are in substantial agreement with the calculation of Ref. 2, which employs a different model distribution function.

The γ, ω, and $k_{\|}$ of the fastest growing mode for each case are tabulated in Table II. These growth rates, though small compared to ω_{ce}, are sufficiently large to lead to significant wave growth in the experimental situation. The theory also predicts the frequency width of the unstable wave spectrum. For example, in Figure 3(d), the $\gamma = 0$ contour spans from $0.22\ \omega_{ce}$ to $0.61\ \omega_{ce}$. The bandwidth of unstable frequencies could be measured in the experiments as a test of this theory. Examining Figures 3(a)-(f) also shows that, as the density is increased, the frequency range of the unstable wave spectrum shifts upward toward ω_{ce}.

The necessary conditions for instability derived in section II are also plotted in Figures 3(a)-(f). In all cases, the positive γ contours indeed lie within these boundaries. This is a convincing verification that the conditions of Table I obtained on the basis of physical arguments are indeed necessary conditions for instability.

All growth rates shown so far in Figures 3(a)-(f) and Table II were obtained from the analytical expressions derived in section IV. In some particular cases, we have verified these results by two-dimensional numerical integration of the Fokker-Planck equation (16). The example shown in Table III compares analytical results with γ calculated using the distribution functions from the two-dimensional numerical calculations. The agreement between the analytical theory and the two-dimensional numerical calculations is satisfactory, confirming that the analytical f can be used with confidence. The satisfactory agreement between the two-dimensional numerical and analytical results is also of some practical computational interest since, in the two-dimensional numerical calculations, the production of plots of the type shown in Figures 3(a)-(f) requires a large amount of computer time. In order to obtain the maximum growth rate in the two-dimensional calculations, and to avoid having to sweep the allowable $(\omega,k_{\|})$-space, we can take for $(\omega,k_{\|})$ the point at which the analytic theory predicts a maximum growth rate. This was done in Table III.

The resonance conditions can be used to further understand certain features of the growth rates and of the unstable regions in $(\omega,k_{\|})$-space. The part of the stability boundary ($\gamma = 0$) along the line $v_{AD} = v_2$ is due to the transition of the anomalous Doppler resonance from the highly anisotropic RF plateau to the nearly isotropic region of velocity space above the plateau, $v_{\|} > v_2$. The growth rate peaks at this boundary and precipitously drops to negative values as v_{AD} exceeds v_2 and γ_{AD} becomes negative, as discussed in section IV. The part of the stability boundary which lies near the line $v_L = v_1$ is due to strong Landau damping in the region of $v_{\|}$ close to the bulk of the distribution function. In the higher density regime, shown in Figures 3(c)-(f), the high frequency part of the stability boundary is principally due

to the rapidly increasing contribution of the Doppler cyclotron resonance damping as $v_{DC} = (\omega - \omega_{ce}/k_{\|})$ moves toward the bulk with increasing ω.

Finally, a point of interest to current drive is that the stability boundary, $\gamma = 0$, does not cross the line $\omega = k_{\|}v_1$. In other words, the unstable spectrum of magnetized plasma waves does not extend below the lower velocity limit of the plateau. This is made clear in Figure 4, where the maximum growth rate at each wave phase velocity is plotted. The growth rate as a function of phase velocity is obtained from the data in Figures 3(a)-(f) by sweeping the line $\omega = v_{ph}k_{\|}$ through the unstable region and selecting the maximum γ for each given value of v_{ph}. In this example, the unstable wave spectrum lies between $4.3 < \omega/k_{\|} < 7.9$, while the plateau extends from $v_1 = 3.95$ to $v_2 = 20.7$. The corresponding $F(v_{\|})$ and $T_{\perp}(v_{\|})$ are shown in Figure 5. This means that quasi-linear diffusion produced at the Landau resonance of these waves will not substantially add to the plateau height, as it might if the unstable wave spectrum extended below v_1. On the other hand, the unstable spectrum may lead to strong quasilinear pitch angle scattering of the particles near $v_{\|} \lesssim v_2$ and this will change the plateau in that region. In the presence of strong RF diffusion, these particles, even though back-scattered in $v_{\|}$ by the unstable fields, can be maintained in the $v_{\|} < v_2$ region of the RF spectrum, and thus continue to contribute to the current. The new steady-state $f_e(v_{\|},v_{\perp})$, in the presence of both the applied RF spectrum and the unstable fields, remains to be determined.

VI. CONCLUSIONS

The above stability and growth rate calculations can easily be applied to assess the stability of the anomalous Doppler mode for any particular set of

experimental conditions, as was done in section V for the Versator II experiment. In the Versator II experiments the relatively large value of $y^2 = \omega_{pe}^2/\omega_{ce}^2 = 1$ admits a comparatively broad frequency spectrum of unstable waves, the upper bound of the frequency spectrum given approximately by $\omega^{max}/\omega_{ce} = y/\sqrt{1 + y^2}$. In other lower-hybrid current drive experiments, y^2 is small; for example, in the PLT[6] and Alcator C[7] experiments, y^2 is typically less than 0.15. The lower values of y^2 tend to be stabilizing for this mode, Eq. (12); therefore, in experiments with low values of y the AD mode is expected to be unstable only in a narrow frequency range, $(v_2/v_1 - 1)^{-1} < \omega/\omega_{ce} < \omega^{max}$, or entirely stable.

The stability of the anomalous Doppler mode for parameters typical of an RF-driven tokamak fusion reactor can also be assessed using the above criteria. The value of $\beta = 2nT/(B^2/2\mu_0)$ turns out to be an important parameter in the stability analysis. In reactor grade plasmas the needed value of β constrains y^2 to be of order 1 or larger. In particular, $\beta = 7\%\ y^2 T_4$, where $T_4 = (T_e + T_i)/2$ is the average temperature in units of 10^4 eV. For a plasma with central β of 14% and average temperature of 10 keV, it follows that $y^2 = 2$. Since relativistic electron energies are projected for efficient current drive in the reactor regime, it will be necessary to use a relativistically correct model electron distribution function to calculate the growth rate of this mode in the RF-driven reactor. The model discussed above for $f(v_\perp, v_\parallel)$ must be extended to relativistic velocities before the reactor problem can be solved. We can, however, apply the relativistic necessary condition for instability, Eq. (15). We consider a sufficient condition for stability obtained by reversing the inequality (15). Taking $y^2 = 2$, the stability condition then depends on the values of v_1 and v_2. For example, if we take $v_1 = 3$, we have $v_2 < 0.8\ c$, or $n_{\parallel_2} > 1.25$ for stability,

decreasing $n_{\|}$ below 1.25, which is desirable for improved current drive efficiency would be a destabilizing influence for the ADI. It is possible, however, that in a hot reactor-grade plasma this mode may be stabilized by increased Landau damping on the thermal bulk. To fully assess the stability of the ADI in the reactor regime, further calculations will be needed, including a relativistically correct distribution function model.

As far as the efficiency of RF current drive is concerned, the ADI will have two main effects. First, the excitation of unstable waves will cause power to be lost from the RF-driven tail at a rate larger than the collisional rate. This power loss will tend to reduce the efficiency of RF current drive. Second, a quasi-linear, perpendicular broadening of the plateau at the anomalous Doppler resonance is expected; hence, the effective perpendicular temperature of the plateau will increase. The increase in $T_{\perp}$ will tend to increase the efficiency of RF current drive. To assess which of these competing effects will be dominant, it will be necessary to solve the full Fokker-Planck/quasi-linear equations, including quasi-linear diffusion caused by the unstable waves. However, as a matter of practical importance, the undesirable effects of the ADI can be eliminated by application of electron cyclotron heating. As seen from Eq. (29), the destabilizing term, $F/(k_{\|}T_{\perp})$, can be reduced by increasing $T_{\perp}$, which could be accomplished by ECRH.

APPENDIX

Here we evaluate the quantity $\partial \mathrm{Re}(D)/\partial\omega\big|_{\mathrm{Re}(D)=0}$, which appears in the growth rate of the electrostatic wave, Eq. (4). We have, from Eq. (1):

$$\mathrm{Re}(D) = 1 - \frac{k_\perp^2}{k^2}\frac{\omega_{pe}^2}{\omega^2 - \omega_{ce}^2} - \frac{\omega_{pe}^2}{\omega^2}\frac{k_\parallel^2}{k^2} \tag{45}$$

and:

$$\frac{\partial \mathrm{Re}(D)}{\partial\omega} = \frac{2\omega\, k_\perp^2\, \omega_{pe}^2}{k^2(\omega^2 - \omega_{ce}^2)} + \frac{2\,\omega_{pe}^2\, k_\parallel^2}{\omega^3 k^2} \tag{46}$$

Considering the root of Eqn. (45), $\omega^2 = (k_\parallel^2/k^2)\, y^2/(1 + y^2)$, where $y^2 = \omega_{pe}^2/\omega_{ce}^2$, and neglecting ω^2/ω_{UH}^2, where $\omega_{UH}^2 = \omega_{pe}^2 + \omega_{ce}^2$ is the upper hybrid resonance frequency, then from Eqs. (45) and (46) we find

$$\frac{\partial \mathrm{Re}(D)}{\partial\omega}\bigg|_{\mathrm{Re}(D)=0} = \left[1 - \frac{\omega_{pe}^2}{\omega^2}\frac{k_\parallel^2}{k^2}\right]\frac{2\omega}{\omega^2 - \omega_{ce}^2} + \frac{2\,\omega_{pe}^2\, k_\parallel^2}{\omega^3 k^2}, \tag{47}$$

so that

$$\frac{\partial \mathrm{Re}(D)}{\partial\omega}\bigg|_{\mathrm{Re}(D)=0} = \frac{2}{\omega}\left[\frac{1 + y^2 - \omega^2/\omega_{ce}^2}{1 - \omega^2/\omega_{ce}^2}\right]. \tag{48}$$

ACKNOWLEDGMENTS

This work was supported in part by DOE Contract No. DE-AC02-78ET-51013 and in part by Hydro-Quebec Project No. 01844-571-59535.

REFERENCES

1. H. Knoepfel and D.A. Spong, Nucl. Fusion 19, 785 (1979).

2. S.C. Luckhardt in Radiofrequency Plasma Heating, AIP Conference Proceedings No. 129, ed. D.G. Swanson, American Institute of Physics, New York p. 158 (1985).

3. V. Fuchs, R.A. Cairns, M.M. Shoucri, K. Hizanidis, and A. Bers, Phys. Fluids 28, 3619 (1985).

4. N. Krall and A. Trivelpiece, Principles of Plasma Physics, McGraw-Hill, New York (1973).

5. M. Mayberry, M. Porkolab, K. Chen, A. Fisher, D. Griffin, R. Kaplan, S. Luckhardt, J. Ramos, and R. Rohatgi, Phys. Rev. Lett 55, 829 (1985).

6. S. Bernabei et al., Phys. Rev. Lett. 49, 1255 (1982).

7. M. Porkolab et al., Phys. Rev. Lett. 53, 450 (1984).

TABLE I

Necessary Conditions for Instability

Landau resonance on plateau	$\omega \geq v_1 k_{\|}$
A.D. resonance on plateau	$\omega \leq v_2 k_{\|} - 1$
D.C. resonance out of bulk	$\omega < 1 - v_1 k_{\|}$
Dispersion relation	$\omega < \frac{y}{(1 + y^2)^{1/2}}$

TABLE II

Versator II Experimental and Theoretical Parameters for a Density Scan -- the Maximum Growth Rate γ_{max}, and the Corresponding ω and $k_{\|}$

	Versator II Conditions				Theory of LHCD[3]			Maximum Growth Rate		
Case	n_e	v_2^{ACC}	J	y^2	v_1	T_p	F_p	γ_{max}	$\omega^{(m)}$	$k_{\|}^{(m)}$
a	0.4×10^{13}	30.4	1.0	0.278	4.0	117	2.16×10^{-3}	1.26×10^{-3}	0.29	4.2×10^{-2}
b	0.6	27.5	0.68	0.417	4.0	101	1.8	1.54	0.34	4.8
c	0.8	25.4	0.51	0.556	4.0	90	1.58	1.713	0.37	5.3
d	1.0	23.8	0.41	0.694	4.0	82	1.44	1.825	0.38	5.8
e	1.5	20.7	0.27	1.04	3.9	66	1.26	2.043	0.44	6.9
f	2.0	18.7	0.2	1.39	3.9	57	1.14	2.165	0.47	7.8

T_{bulk} = 200 eV, B = 1.2 Tesla, Z_{eff} = 3

TABLE III

Comparison of Some Two-Dimensional Numerical Results

with Additional Analytical Theory

Spectrum Location v_1, v_2	y^2	Two-Dimensional Numerical			Theory		
		γ_{max}	γ_{AD}	γ_L	γ_{max}	γ_{AD}	γ_L
4, 19	0.8	0.51×10^{-3}	0.62×10^{-3}	-0.113×10^{-3}	0.64×10^{-3}	0.72×10^{-3}	-0.076×10^{-3}
4, 19	1.2	0.81	0.93	-0.153	1.01	1.14	-0.112
4, 19	2.25	1.6	1.87	-0.273	2.0	2.1	0.176

FIGURE CAPTIONS

Figure 1. Two-dimensional distribution function for RF current drive, and velocity space resonances for Landau damping, anomalous Doppler resonance, and Doppler cyclotron resonance.

Figure 2. Necessary conditions for instability in $(\omega,k_{\|})$-space: $v_L = \omega/k_{\|}$, the Landau velocity; $v_{AD} = (\omega_{ce} + \omega)/k_{\|}$, the anomalous Doppler resonance velocity; and $v_{DC} = (\omega - \omega_{ce})/k_{\|}$, the Doppler cyclotron resonance velocity. ω^{max} is the maximum frequency allowed by the wave dispersion relation. The condition that v_2 equals the relativistic anomalous Doppler resonance is indicated by the dashed line.

Figure 3. (a)-(f) Plots of the growth rate, γ, and the necessary conditions for instability, with y^2 as a parameter for the conditions in Table II.

Figure 4. Plot of $\gamma_{max}(\omega/k_{\|})$ and $F(v_{\|})$ for the case where $y^2 = 1.04$, $v_1 = 3.95$, and $v_2 = 20.7$.

Figure 5. Numerical $F(v_{\|})$ and $T_{\perp}(v_{\|})$ obtained from numerical solution of the two-dimensional Fokker-Planck equation. $D = D_{QL}/(\nu_e v_e^2)$, $Z=Z_i$ the ion charge state, and J is the current density in units of $en_e v_e$.

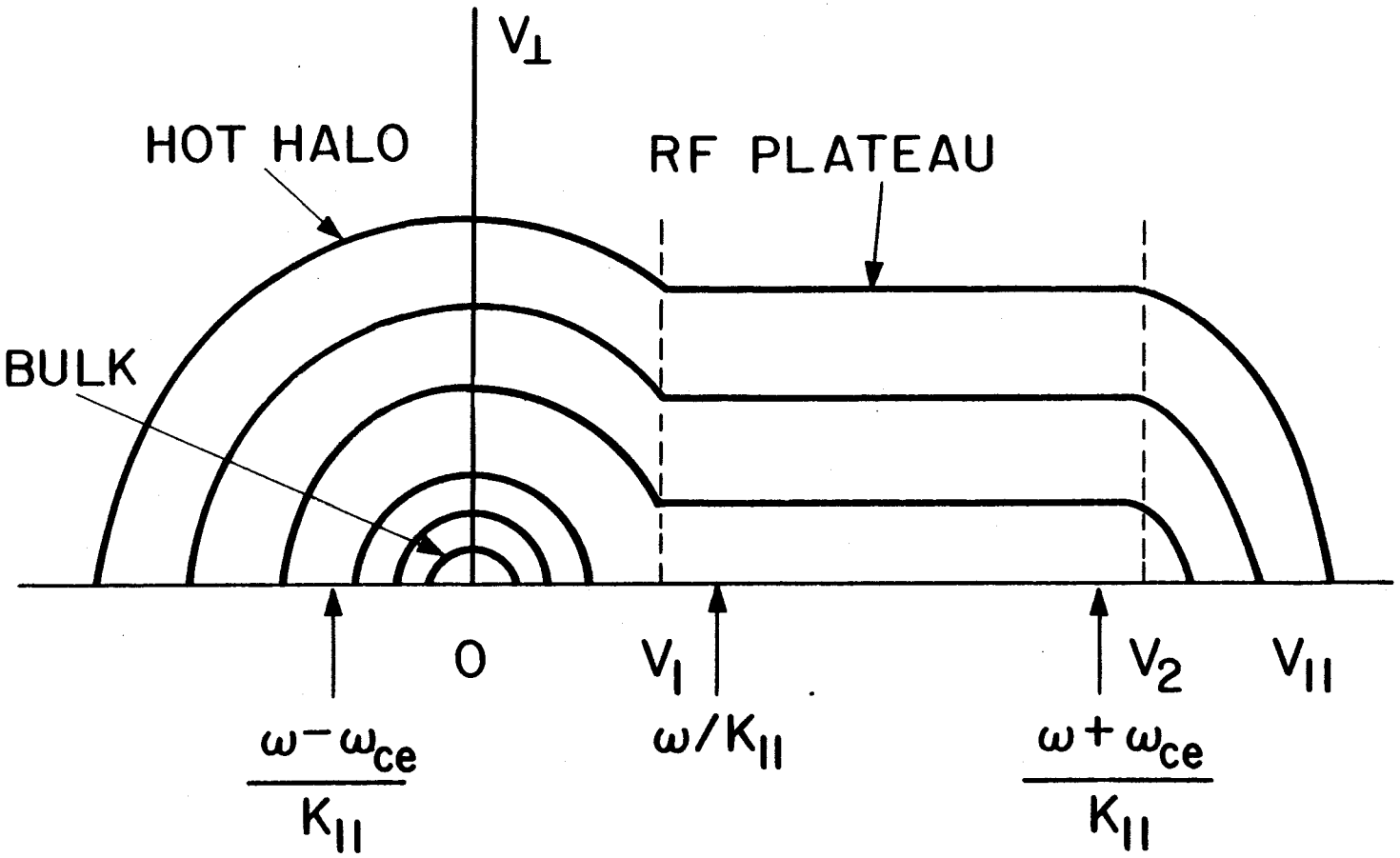

Fig. 1
Luckhardt et al

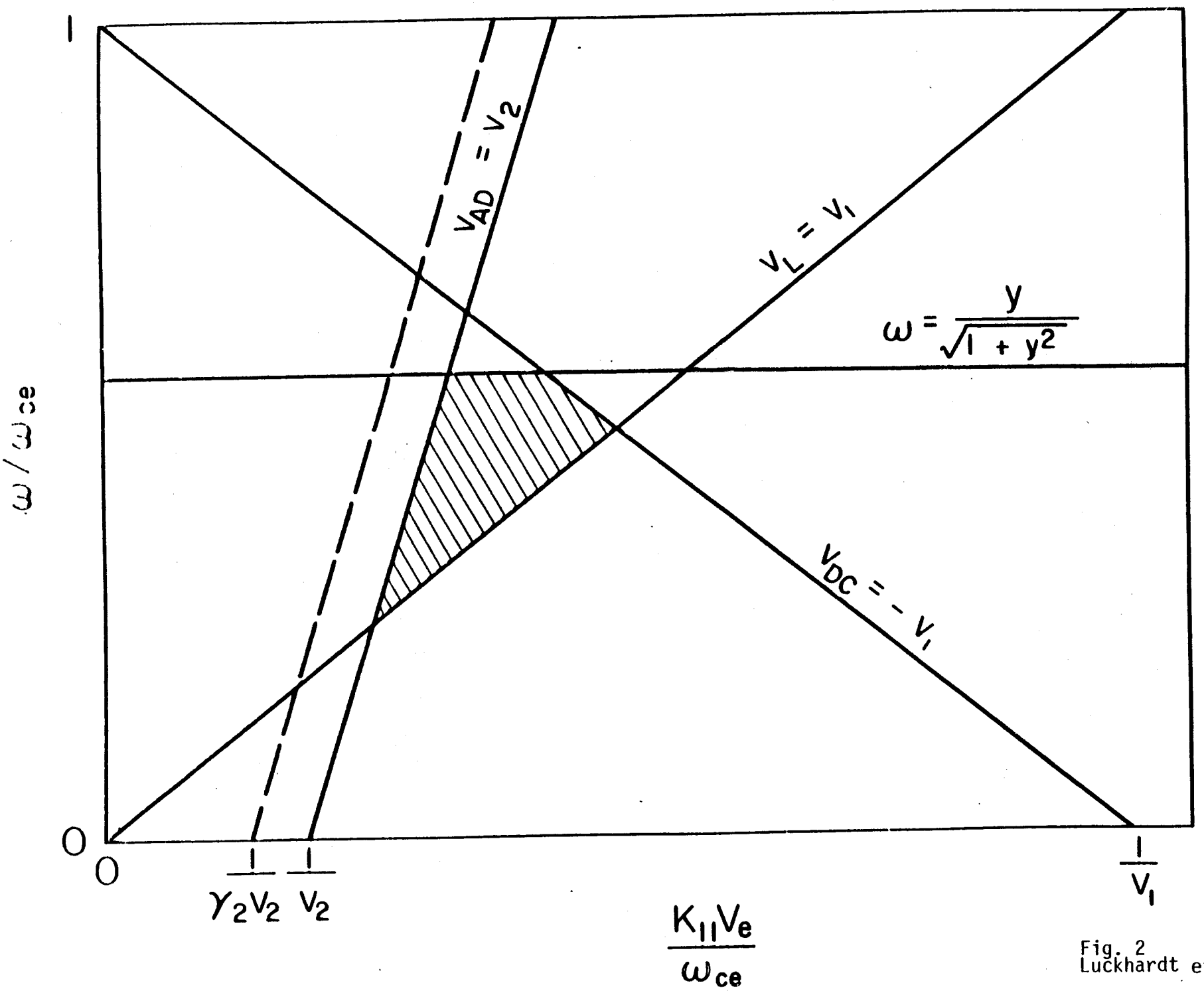

Fig. 2
Luckhardt et al

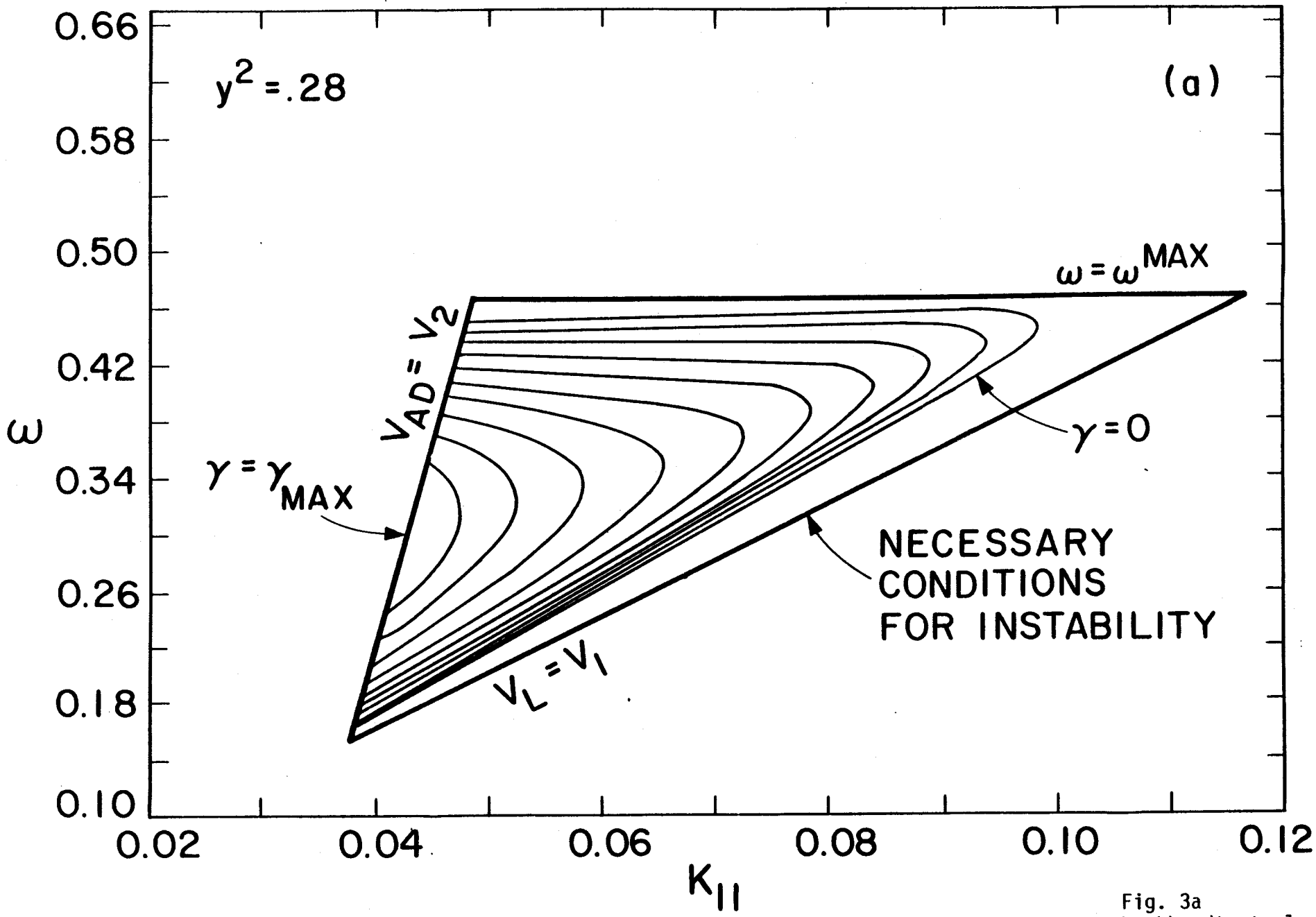

Fig. 3a
Luckhardt et al

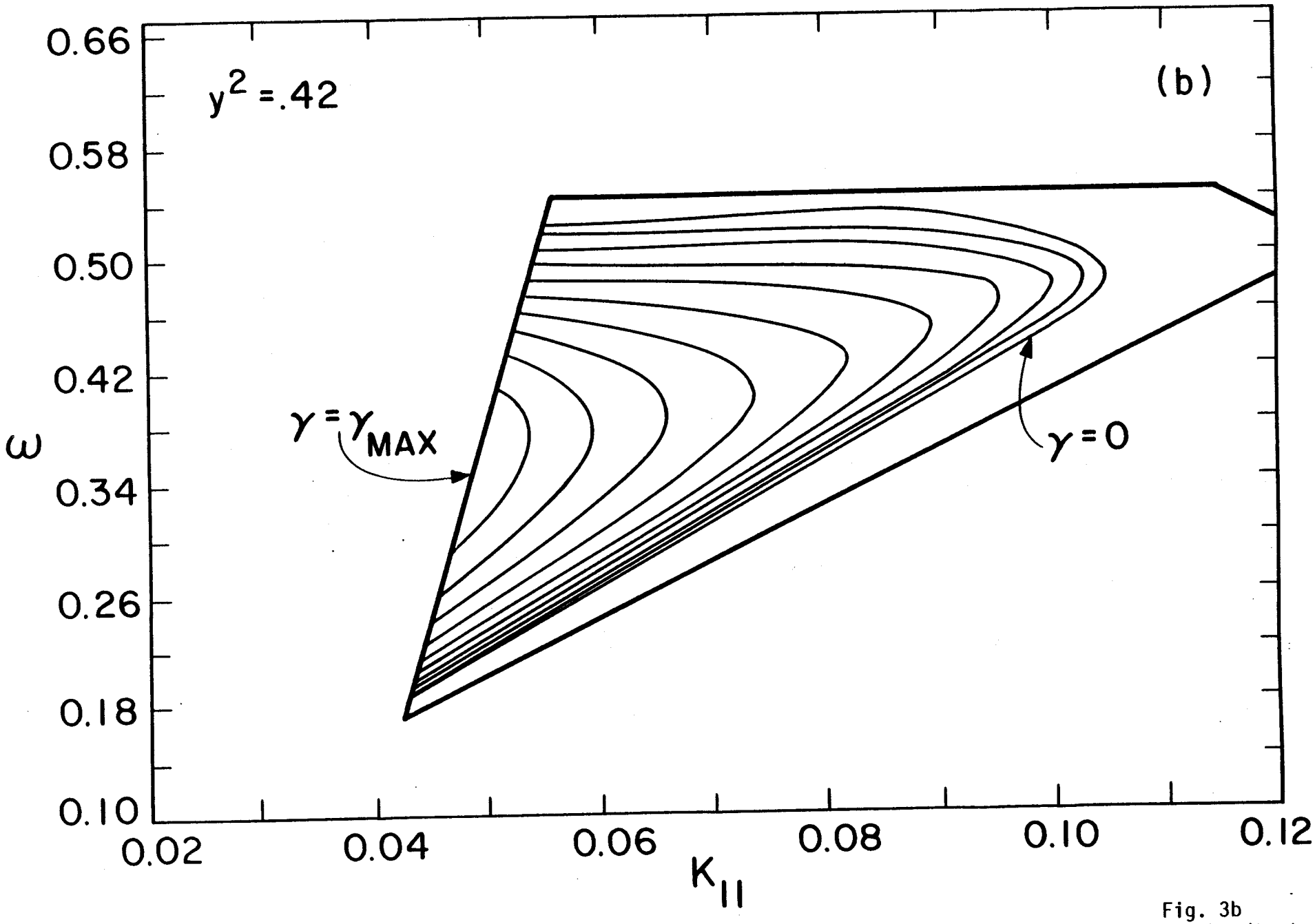

Fig. 3b
Luckhardt et al

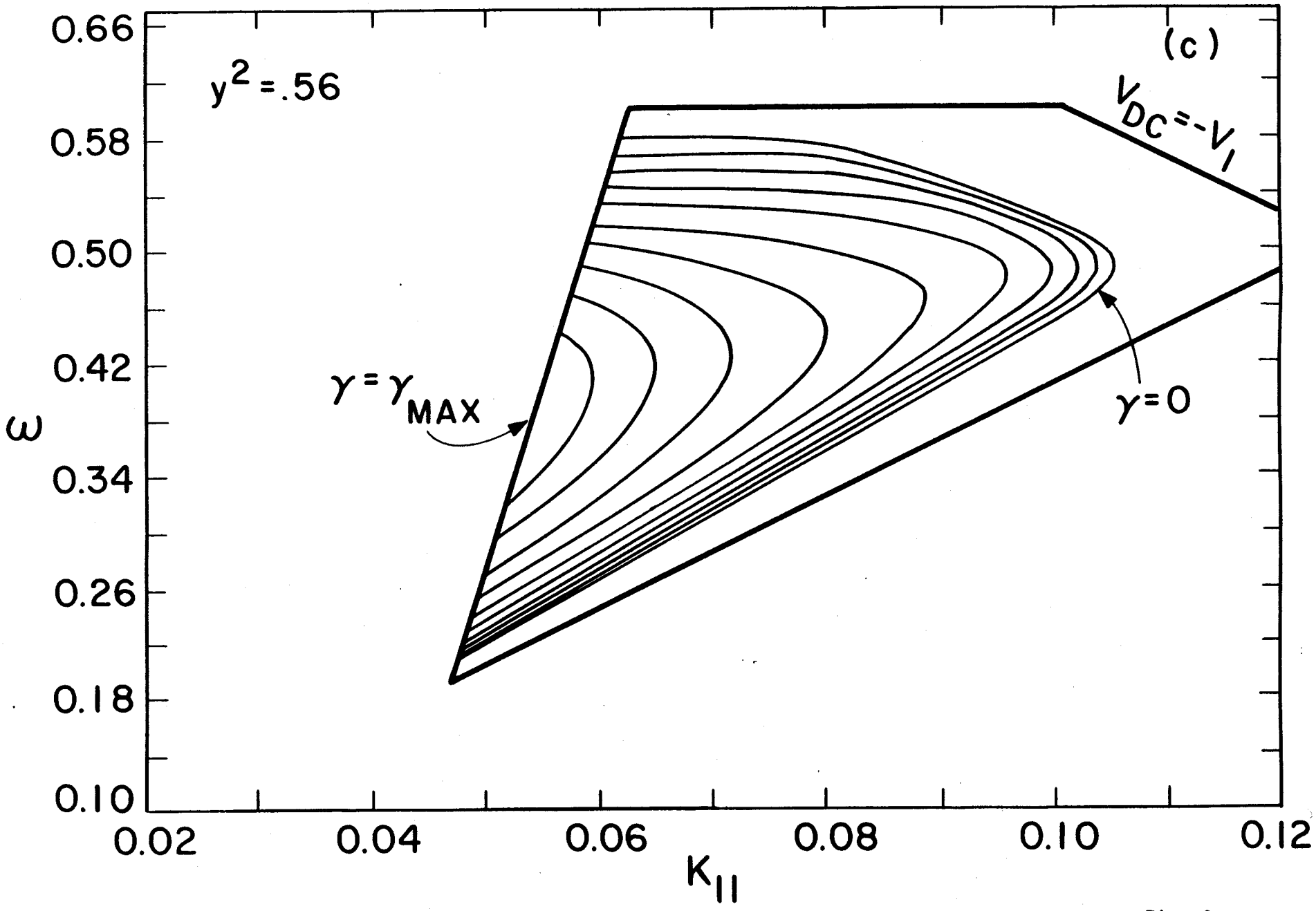

Fig. 3c
Luckhardt et al

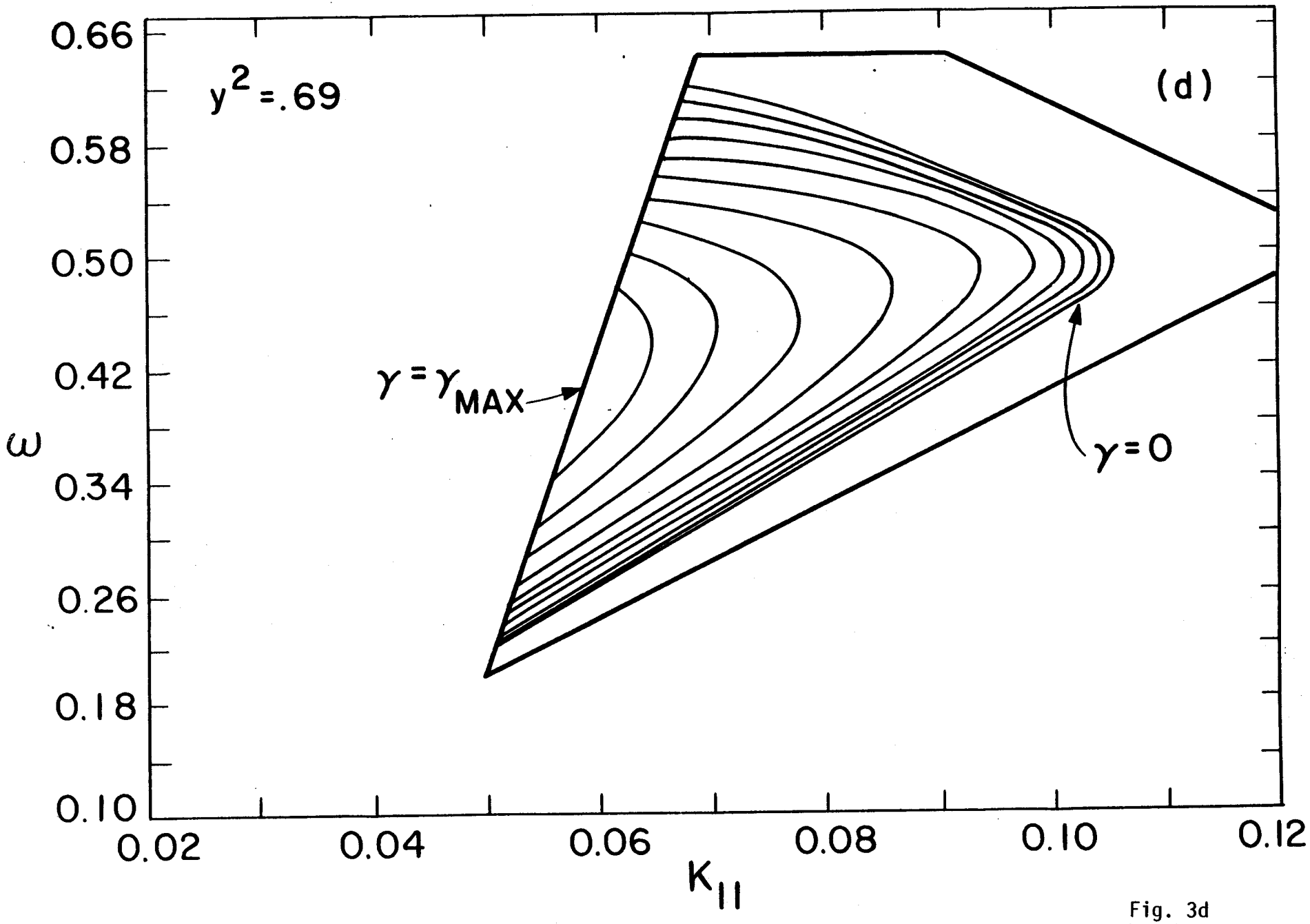

Fig. 3d
Luckhardt et al

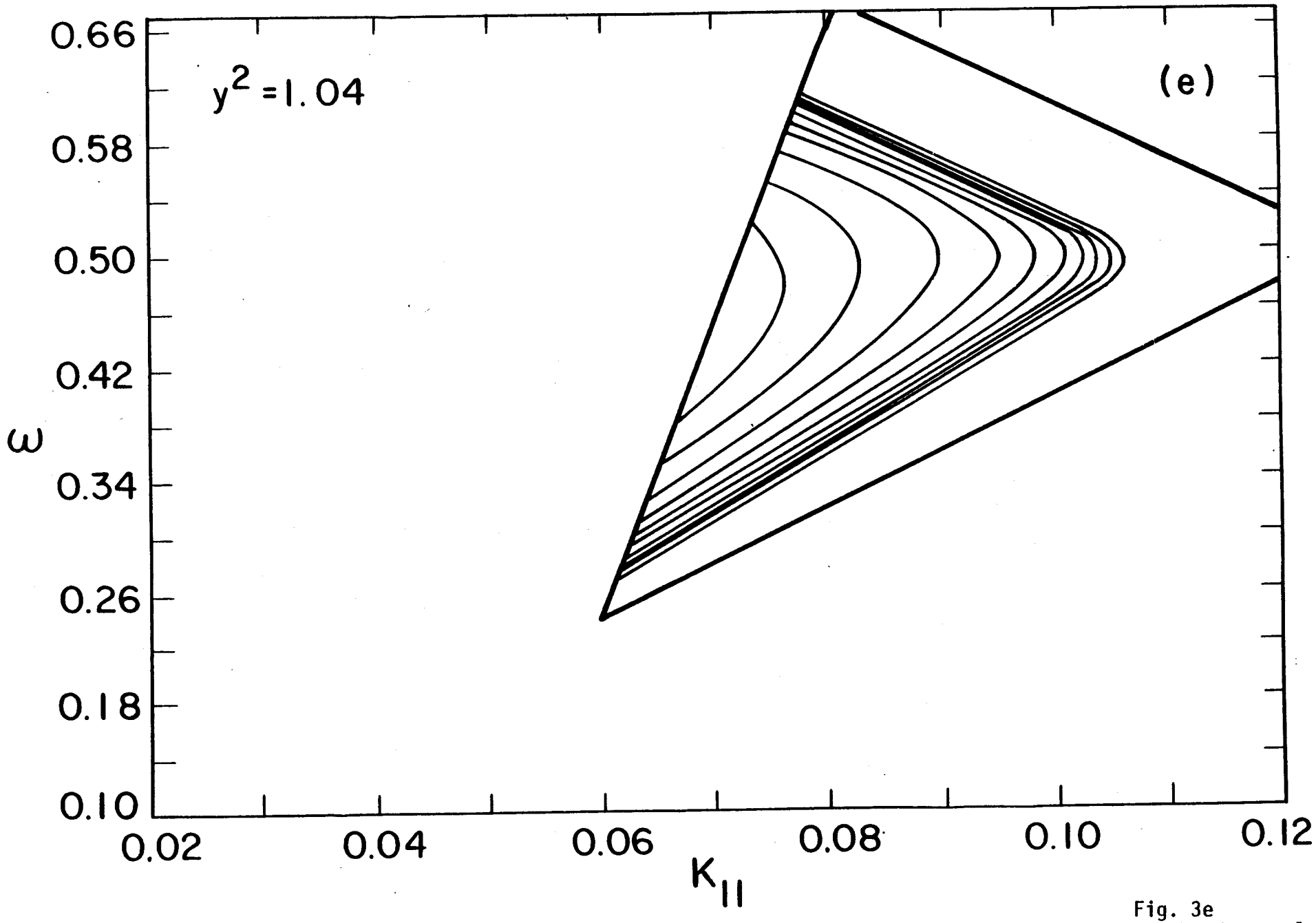

Fig. 3e
Luckhardt et al

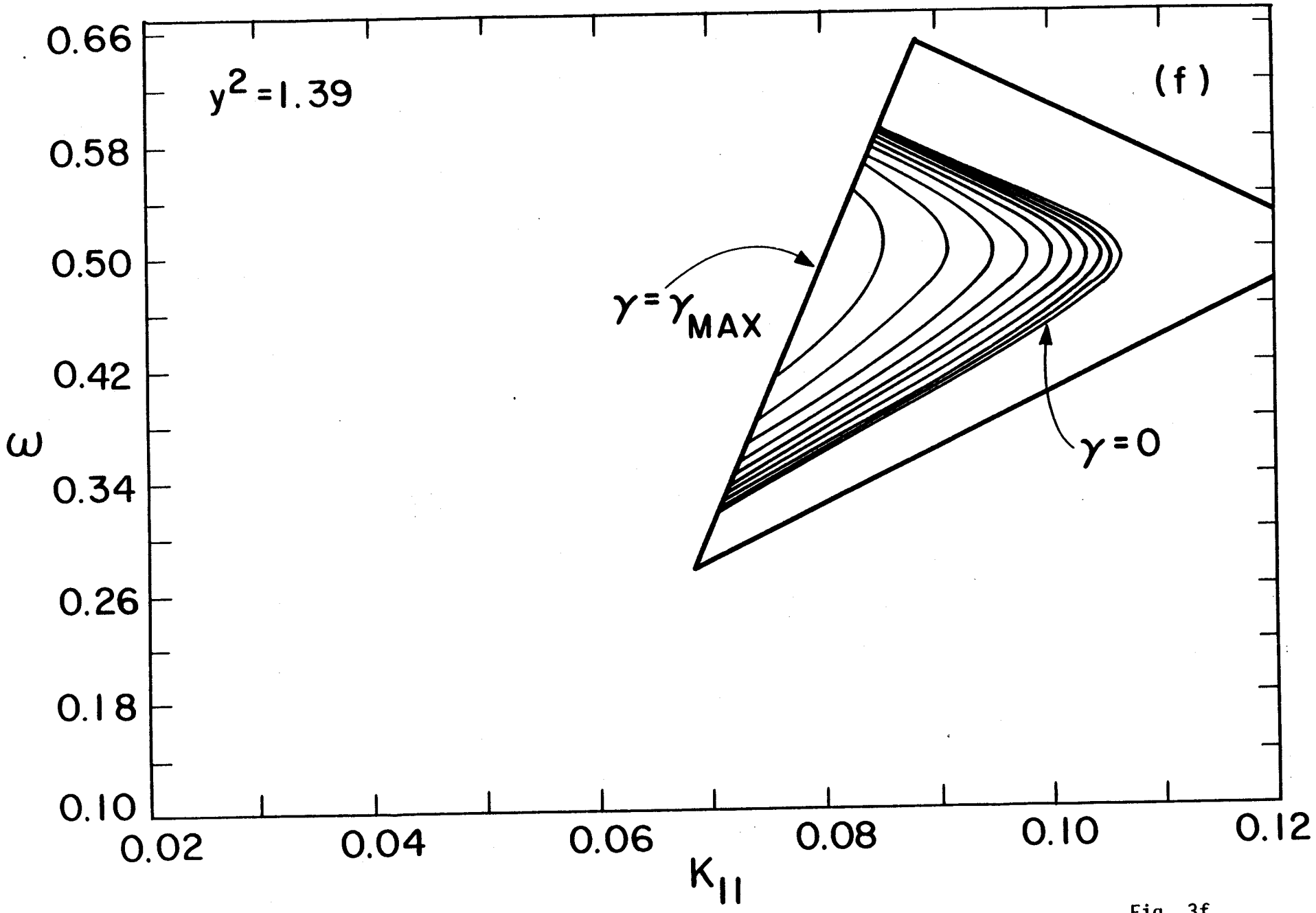

Fig. 3f
Luckhardt et al

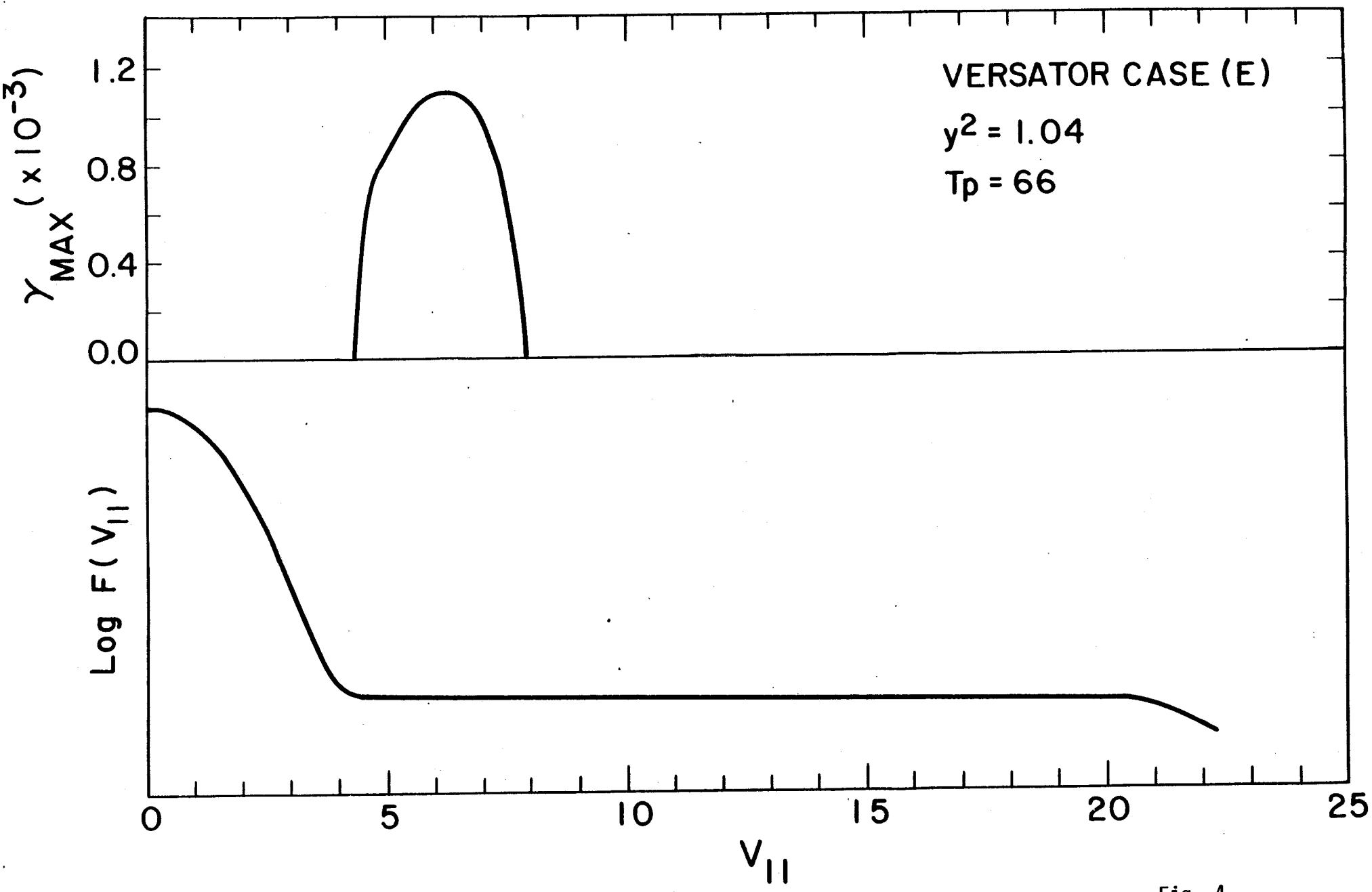

Fig. 4
Luckhardt et al

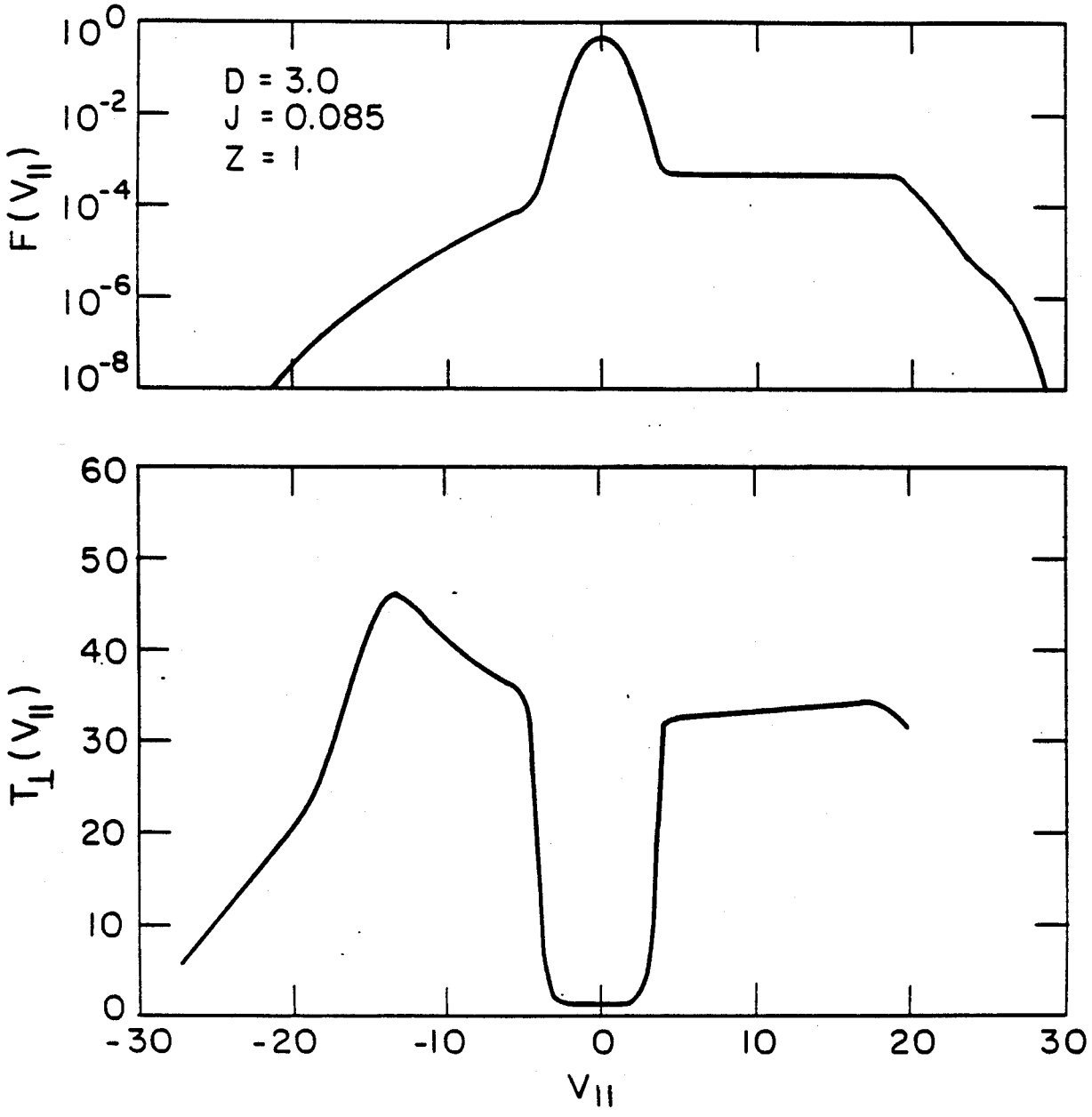
D = 3.0
J = 0.085
Z = 1
10^0
10^{-2}
10^{-4}
10^{-6}
10^{-8}
$F(V_{||})$
60
50
40
30
20
10
0
$T_\perp(V_{||})$
-30
-20
-10
0
10
20
30
$V_{||}$

Fig. 5